

LETTER TO THE EDITOR

Mid-infrared evolution of η Car from 1968 to 2018^{*},

A. Mehner¹, W.-J. de Wit¹, D. Asmus², P.W. Morris³, C. Agliozzo⁴, M.J. Barlow⁵, T.R. Gull⁶, D.J. Hillier⁷, and G. Weigelt⁸

¹ ESO – European Organisation for Astronomical Research in the Southern Hemisphere, Alonso de Cordova 3107, Vitacura, Santiago de Chile, Chile

² Department of Physics & Astronomy, University of Southampton, Southampton, SO17 1BJ, UK

³ California Institute of Technology, IPAC, M/C 100-22, Pasadena, CA 91125, USA

⁴ ESO – European Organisation for Astronomical Research in the Southern Hemisphere, Karl-Schwarzschild-Straße 2, 85748 Garching, Germany

⁵ Department of Physics & Astronomy, University College London, Gower Street, London WC1E 6BT, UK

⁶ NASA Goddard Space Flight Center, Code 667, Greenbelt, MD 20771, USA

⁷ Department of Physics & Astronomy, University of Pittsburgh, 3941 O’Hara Street, Pittsburgh, PA 15260, USA

⁸ Max Planck Institute for Radio Astronomy, Auf dem Hügel 69, 53121, Bonn, Germany

August 27, 2019

ABSTRACT

Eta Car is one of the most luminous and massive stars in our Galaxy and is the brightest mid-infrared (mid-IR) source in the sky, outside our solar system. Since the late 1990s the central source has dramatically brightened at ultraviolet and optical wavelengths. This might be explained by a decrease in circumstellar dust extinction. We aim to establish the mid-IR flux evolution and further our understanding of the star’s ultraviolet and optical brightening. Mid-IR images from 8 – 20 μm were obtained in 2018 with VISIR at the Very Large Telescope. Archival data from 2003 and 2005 are retrieved from the ESO Science Archive Facility and historical records are collected from publications. We present the highest angular resolution mid-IR images of η Car to date at the corresponding wavelengths ($\geq 0.22''$). We reconstruct the mid-IR evolution of the spectral energy distribution of the spatially integrated Homunculus nebula from 1968 to 2018 and find no long-term changes. Eta Car’s bolometric luminosity has been stable over the past five decades. We do not observe a long-term decrease in the mid-IR flux densities that could be associated with the brightening at ultraviolet and optical wavelengths, but circumstellar dust must be declining in our line-of-sight only. Short-term flux variations within about 25% of the mean levels could be present.

Key words. circumstellar matter – Stars: individual: eta Car – Stars: massive – Stars: mass-loss – Stars: variables: S Doradus – Stars: winds, outflows

1. Introduction

Eta Car is the archetype of unstable massive stars, eruptive mass loss, supernova (SN) impostors, and a reference for understanding the precursor eruptions that lead to superluminous SNe. The star has a current mass of about $100 M_{\odot}$ and is in an eccentric binary system (Damineli et al. 1997, Davidson & Humphreys 2012 and references therein). During an eruptive event in the 19th century (see Frew 2004 for the historical lightcurve), the system ejected $\geq 45 M_{\odot}$ of material (Morris et al. 2017; see also Smith et al. 2003), forming the bipolar Homunculus nebula.

Eta Car is often described as an extreme case of a Luminous Blue Variable (LBV). LBVs are evolved massive stars with initial masses $\geq 20 M_{\odot}$ that exhibit instabilities that are not understood, resulting in enhanced mass loss (Conti 1984; 1997, Humphreys & Davidson 1994, Nota & Lamers 1997). They have been considered to be stars in transition to the Wolf-Rayet stage (e.g., Maeder 1983, Langer et al. 1994), but more recent observational and theoretical work suggests that some LBVs could be the immediate progenitors of SNe (e.g., Kotak & Vink 2006,

Trundle et al. 2008, Gal-Yam & Leonard 2009, Smith et al. 2007, Groh et al. 2013).

A crucial parameter for understanding η Car is the luminosity since this provides a mass estimate via the Eddington limit. Most of η Car’s visible and ultraviolet (UV) light is absorbed by circumstellar dust and re-radiated in the infrared (IR; Davidson 1971, Davidson & Ostriker 1972, Pagel 1969, Westphal & Neugebauer 1969, Robinson et al. 1973, Sutton et al. 1974). The star’s luminosity can thus be obtained from the IR spectral energy distribution (SED). Eta Car is unparalleled as an IR radiation source and its brightness makes observations with sensitive IR satellite instrumentation impossible. Most of the $0.25 - 0.44 M_{\odot}$ of cool dust is located in the central $5''$ region in a “disrupted” equatorial structure (Morris et al. 1999; 2017), also referred to as the “Butterfly” nebula (Chesneau et al. 2005). Early estimates of η Car’s total luminosity are on the order of $L = 5 \times 10^6 L_{\odot}$ (Neugebauer & Westphal 1968, Westphal & Neugebauer 1969, Pagel 1969, Robinson et al. 1973, Sutton et al. 1974, Cox et al. 1995, Davidson & Humphreys 1997). Morris et al. (2017) conclude that η Car’s total luminosity in the 1970s was $L = 4.1 \times 10^6 L_{\odot}$, for the commonly adopted distance of 2.3 kpc. A distance revision to 2.6 kpc could imply a 25 – 30%

^{*} Based on observations collected at ESO’s Very Large Telescope under Prog-IDs: 074.A-9016(A), 0101.D-0077(A). Based on observations made with ESO Telescopes at the La Silla Paranal Observatory under Prog-IDs: 60.A-9126(A,C,E,I), 69.D-0304(B), 71.D-0049(A).

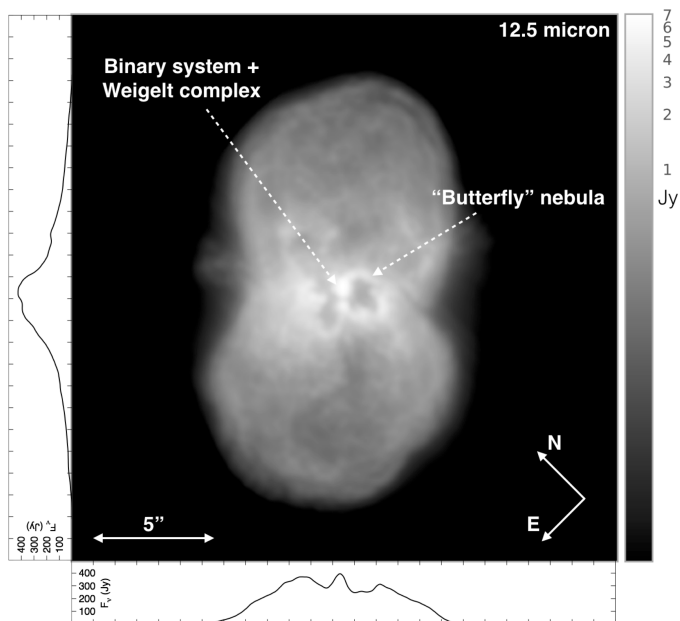


Fig. 1: VISIR image of the Homunculus nebula at $12.5 \mu\text{m}$ in 2018, tracing the thermal emission from heated dust and the H α 7-6 emission. The field-of-view is $25'' \times 25''$, the spatial resolution is $0.3''$. The flux density in Jy per detector pixel ($0.045''/\text{pixel}$) is shown as well as the integrated flux along the image axes. The brightest knot in the center of the nebula is due to a shell surrounding the star, an inner torus or disk, or a pinwheel structure, and includes the Weigelt complex (Weigelt & Ebersberger 1986). The two bright loops form the “Butterfly” nebula, where 50% of the integrated flux originates from.

increase in luminosity (Davidson et al. 2018a). The luminosity of the secondary star is a factor of 10 lower (Mehner et al. 2010).

Some authors have suggested a change in the mid-IR flux since the 1970s. Russell et al. (1987) reported a 30% decrease in the $10.5 \mu\text{m}$ silicate emission compared to values for the 1970s. Smith et al. (1995) found a significant decrease in mid-IR flux in the 1990s compared to the 1970s. Morris et al. (2017) derive a total luminosity of $L = 3.0 \times 10^6 L_{\odot}$ for the 1990s, a decline of 25% in 20 yr. They argue that the decline in mid-IR flux indicates a reduction in circumstellar extinction either by the expansion of dust “shells” or dust destruction. This could cause the simultaneous brightening at UV and optical wavelengths (Davidson et al. 1999; 2005; Martin et al. 2006).

We present newly obtained and previously unpublished mid-IR observations, which are the basis of a re-evaluation of η Car’s mid-IR evolution from 1968 to 2018. In Section 2 we describe the new mid-IR images. We present our findings and re-analyze η Car’s SED over a period of 50 years in Section 3. In Section 4 we conclude that η Car has not undergone any appreciable long-term luminosity changes during this period.

2. Mid-IR observations in 2005 and 2018 with VISIR and in 2003 with TIMM2

Eta Car was observed in 2018 with the upgraded VLT imager and spectrometer for the mid-IR (VISIR; Lagage et al. 2004, Käuffl et al. 2015). The VISIR AQUARIUS detector provides a field of view of $38.0'' \times 38.0''$ with a pixel scale of $0.045''$. We sampled the mid-IR wavelength range with several filters from $7.8 - 19.5 \mu\text{m}$, see Table 1, Table B.1, and Figure A.1. The obser-

Table 1: Mid-IR flux densities of η Car’s spatially integrated Homunculus nebula (2003–2018).

Filter	Wavelength (μm)	Date	Flux density (Jy)	Error flux density ^a (Jy)
VISIR				
J7.9	7.78	2018-05-21	9648	30
PAH1	8.59	2018-04-28	19280	40
ArIII	8.99	2018-12-10	31140	80
SIV_1	9.82	2018-05-21	51030	220
SIV	10.49	2018-04-29	54520	160
PAH2	11.25	2018-12-10	66660	210
B12.4	12.47	2018-04-29	53930	230
NeII	12.81	2018-12-10	63120	470
NeII_2	13.04	2018-12-10	58410	450
Q1	17.65	2018-05-11	93040	2690
Q2	18.72	2018-05-11	100810	3550
Q3	19.50	2018-05-11	97380	9940
PAH2	11.25	2005-01-23	61350	390
NeII ^b	12.81	2005-01-23	44420	1050
TIMM2 ^c				
M	4.6	2003	3590	1230
N7.9	7.9	2003	13260	3880
N8.9	8.7	2003	23650	7810
N9.8	9.6	2003	40590	2840
N10.4	10.3	2003	47710	5060
N11.9	11.6	2003	63360	6980
N12.9	12.3	2003	60000	6100
[NeII]	12.8	2003	80960	8170
Q1	17.8	2003	122190	15190

^a Formal errors from the flux calibration. Systematic uncertainties due to sky variability and detector artifacts can be larger than 10% for N band and 20% for Q band.

^b Observations are strongly impacted by ghosts.

^c Average of observations in January, March, and May 2003. The data are badly affected by stripe patterns.

ervations were carried out at an airmass below 1.3 and at a precipitable water vapor between 1.2 – 3.5 mm, ensuring good image quality. The burst read-out mode was used, which results in a large number of short exposure images with instantaneous point spread functions, corresponding to the momentary atmospheric turbulence. High spatial resolution images can be obtained by re-centering and adding the individual short-exposure images. We reach spatial resolutions close to the diffraction limits in the given filters, namely $0.25 - 0.30''$ in N band and $\sim 0.50''$ in Q band. For the flux calibration, the science observations were either preceded or followed by a mid-IR standard star (HD89682; Cohen et al. 1999) obtained with the same setup as the science observations.

The data reduction was performed with a custom-made PYTHON pipeline. The photometry was determined using classical aperture photometry with an aperture radius of $11''$, which encompasses the entire Homunculus nebula. VISIR absolute flux calibration is accurate to 10% in the N band and 20% in the Q band. The dominating source of uncertainty is the mid-IR sky variability. The count levels in the central bright core of the Homunculus nebula ($1''$ in diameter, see Figure 1) are outside the linear regime for most filters, which implies that we may be underestimating the total flux by a few percent. We do not attempt to correct for this, because longward of $8 \mu\text{m}$ less than 10% and longward of $10 \mu\text{m}$ less than 5% of the flux is produced by this

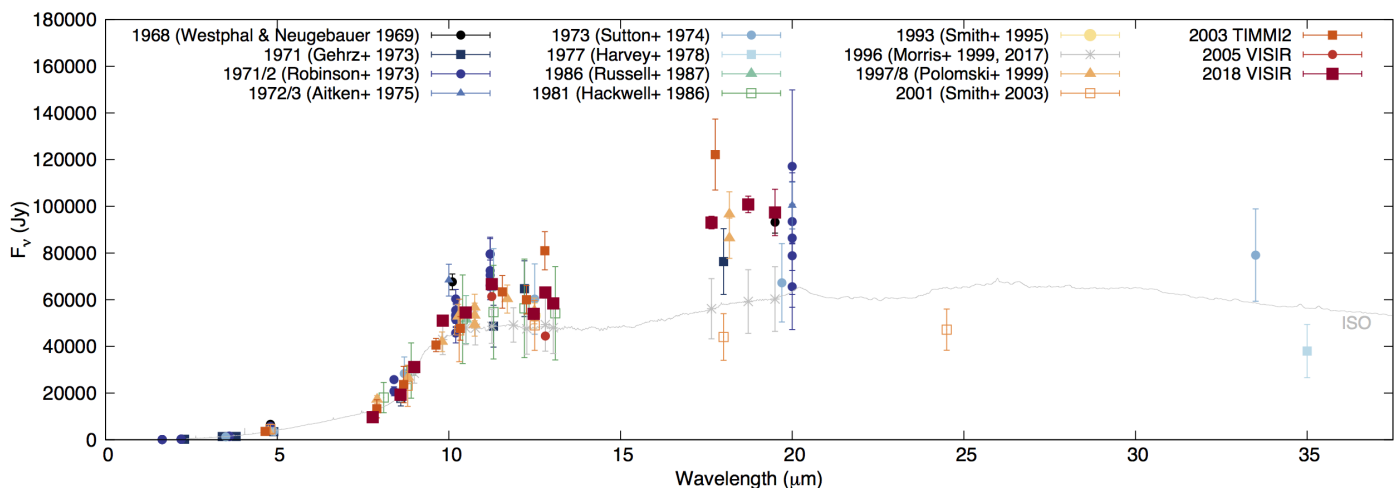


Fig. 2: Mid-IR photometry of the integrated Homunculus nebula from 1968 to 2018. Colored symbols represent our new and historic mid-IR measurements performed in the 1960s (Westphal & Neugebauer 1969), 1970s (Gehrz et al. 1973, Robinson et al. 1973, Aitken & Jones 1975, Sutton et al. 1974, Harvey et al. 1978), 1980s (Hackwell et al. 1986, Russell et al. 1987), 1990s (Smith et al. 1995, Polomski et al. 1999, Morris et al. 1999; 2017), and 2000s (Smith et al. 2003). Calibration uncertainties may be larger than reported due to unaccounted systematic uncertainties, sky variability, detector artifacts, and partial saturation. Open symbols represent values estimated from isophotal contour maps (Hackwell et al. 1986, Smith et al. 2003).

central core. The resulting mid-infrared spectral flux densities and statistical uncertainties are listed in Table 1.

In what follows, we reconstruct the mid-IR SED with our 2018 observations and literature data (references are provided in the caption of Figure 2). In order to be as complete as possible, we also make use of mid-IR images in the ESO Science Archive Facility with unpublished photometry.¹ η Car was observed with VISIR in 2005 in the filters PAH1, PAH2, NeII, and Q2 with the former Boeing detector. Standard star observations were only obtained in the filters PAH2 and NeII, see Table B.1. The pixel scale is $0.075''$ and the images have spatial resolutions of $\sim 0.35''$. Detector artifacts, such as strong striping and ghosts, result in poor flux measurements. In January, March, and May 2003, η Car was observed with the Thermal infrared Multi-Mode instrument (TIMM12, Reimann et al. 2000) at the La Silla 3.6-m Telescope, see Table B.2. The TIMM12 array shows smear and stripe patterns for bright sources, which lead to large errors in the flux calibration. We have averaged the flux values of all TIMM12 observations and present the standard deviation as errors in Table 1. The TIMM12 data should be interpreted with caution.

3. Results

3.1. η Car's flux evolution in the mid-IR

Figure 2 compares the 2018 mid-IR photometry from our VISIR images with previous observations in the period 1968–2005. Figure 3 displays the time evolution of four mid-IR wavelength regions over 50 years and their averages. With a few exceptions, individual values are consistent with each other within 1σ (22% for M band, 13% for N band, and 19% for Q band) of the average. The figures demonstrate long-term stability of the mid-IR flux between 5 and $20\ \mu\text{m}$ over 50 years within the uncertainty of mid-IR flux calibration.

The timescales for the condensation and destruction of dust grains depend on the chemistry and shielding conditions, which are complex in η Car's Homunculus nebula. Ionizing UV and X-

ray radiation escaping from the central binary vary with orbital phase, but we cannot confirm periodic changes in the mid-IR because the observations were obtained at a mix of orbital phases, the orbital coverage is sparse, and the calibration uncertainties are large. The observations in 1971/72 indicate a trend to higher flux values in mid-cycle, similar to what is observed in the radio (White et al. 2005), but Robinson et al. (1973) state that there is no evidence for variations from October 1971 to July 1972 larger than the measurement uncertainties. Polomski et al. (1999) find that the N band and $18\ \mu\text{m}$ flux density increase between March 1997 and November 1998, i.e., around periastron. The emission of the central bright core ($1''$ in diameter) contributes to less than 10% at $8\ \mu\text{m}$, 5% at $10\ \mu\text{m}$, 4% at $13\ \mu\text{m}$, and 2% at $19\ \mu\text{m}$. Any variations due to recent dust formation or destruction close to the star is hidden in the uncertainties of the nebula-encompassing photometry.

Morris et al. (2017) reported that η Car's mid-IR flux decreased by 25% over the last decades.² Their result was based on data obtained in 1996 with the spectrometers onboard the Infrared Space Observatory (ISO; Kessler et al. 1996). While the absolute spectro-photometric calibration of the ISO spectra was hampered by different detector materials with their own signal-dependent susceptibilities to non-linearities and memory effects (e.g., Van Malderen et al. 2004, Morris et al. 2017), the reported decline may be at least partly due to intrinsic orbital variations. A detailed color-temperature analysis with orbital phase will reveal the thermal characteristics of short-term variations, but such a study will require a more homogeneous set of spatial and temporal monitoring observations.

In contrast to Russell et al. (1987), Smith et al. (1995) and Morris et al. (2017), our SED re-construction and investigation of the time evolution does not reveal a noticeable long-term decrease in the mid-IR flux from $8 - 20\ \mu\text{m}$ since the first available

² Morris et al. (2017) display too high values in their figure 7 for the $11\ \mu\text{m}$ photometry by Gehrz et al. (1973) due to a transcription error. Gehrz et al. (1973) contains an inconsistency of a factor of about two between the flux values at $11\ \mu\text{m}$ reported in their table 1 and figure 1. We use the values from their table 1.

¹ <http://archive.eso.org>

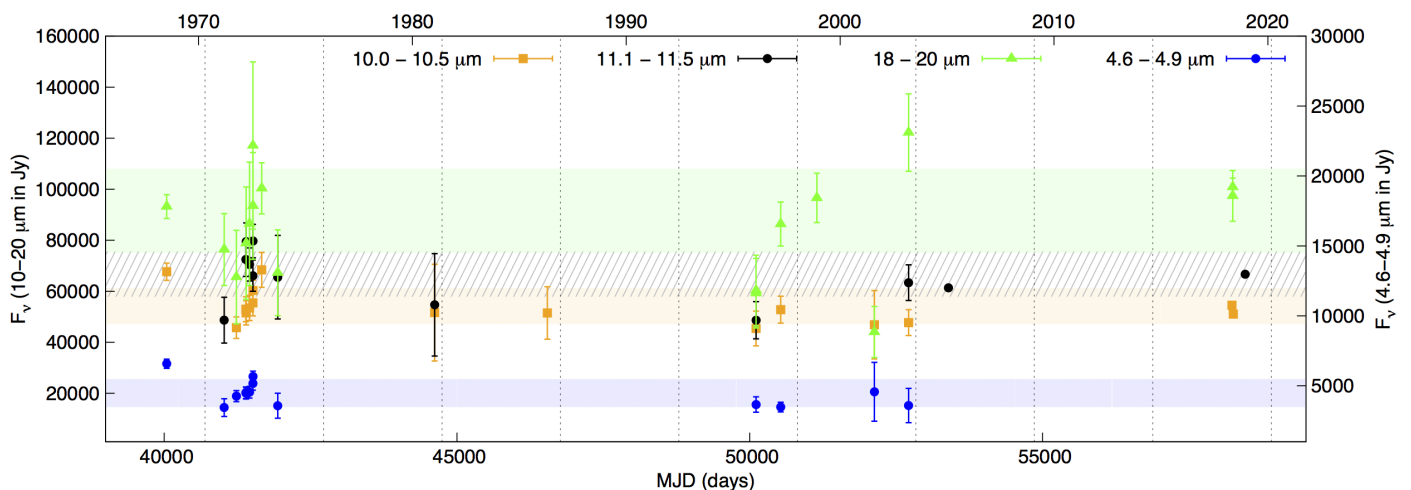


Fig. 3: Time evolution of the mid-IR flux of η Car’s Homunculus nebula from 1968 to 2018 in four wavelength regions, chosen for best temporal coverage. Vertical dashed lines indicate periastron passages. The 1σ region of the average flux for each wavelength region is shown (averages exclude the lower ISO flux values). There is no evidence for a long-term change, but variations with the orbital period cannot be ruled out.

mid-IR photometry in the late 1960s (see Figures 2 and 3). The data support a rather stable mid-IR flux over 50 years, within the large uncertainties of ground-based mid-IR photometry and excluding variations within $\sim 25\%$ of the mean levels. As a consequence, the UV and optical brightening since the late 1990s does not correlate with the integrated mid-IR flux. This is an important finding as the lack of any systematic mid-IR flux change rules out large changes in η Car’s luminosity. We derive a luminosity of about $4.6 \times 10^6 L_{\odot}$ for η Car, using the $2.3 \mu\text{m}$, $3.4 \mu\text{m}$, and $4.9 \mu\text{m}$ photometry of Gehrz et al. (1973), the 2005 and 2018 VISIR mid-IR photometry, and the flux values at $35 - 175 \mu\text{m}$ by Harvey et al. (1978) and at $450 \mu\text{m}$ and $850 \mu\text{m}$ by Gomez et al. (2010).

3.2. On dust extinction

Ever since the 1940s, η Car has brightened steadily at optical wavelengths (Frew 2004) and an accelerated brightening has been observed since the late 1990s (Davidson et al. 1999). Today, η Car at UV and visual wavelengths is more than 2 mag brighter than in the 1990s and the change is remarkably gray (Davidson et al. 2018b, Daminieli et al. 2019). Because η Car is close to the Eddington Limit, in principle this cannot constitute an increase in bolometric luminosity. Davidson et al. (1999; 2005) and Martin et al. (2006) attribute this brightening to a rapid decrease of the circumstellar extinction. The material around η Car is not spherically distributed. The central region is seen through a dust condensation, which strongly attenuates the central source (Hillier & Allen 1992, Weigelt et al. 1995). Davidson et al. (1999) argue that movement of a dusty condensation that intercepts our line-of-sight is unlikely, leaving dust destruction or a decrease of the dust formation rate close to the star as possible explanations. A possible cause may also be small changes in the stellar parameters, which alter the shape of the wind-wind shock cone such that we are no longer looking through the newly formed dust. Daminieli et al. (2019) propose the dissipation of a dusty clump (“coronagraph”) in our line-of-sight.

The variability in the near-IR from 1972–2013 was studied by Whitelock et al. (2004) and Mehner et al. (2014). The star shows a long-term brightening in *JHK*, whereas the *L*-band

emission remains basically constant. The $4 - 8 \mu\text{m}$ flux also shows no long-term variation (Russell et al. 1987; Figure 3). Given that longward of $4 \mu\text{m}$ thermal radiation dominates the SED rather than extinction, one would expect a significant decrease in flux in the $10 - 20 \mu\text{m}$ range only in case of a net destruction of warm ($\sim 200 \text{ K}$) dust grains. Nonetheless, Figure 3 indicates a short-term increase in emission levels during mid-cycle in the 1970s and during periastron in 1998.

The extinction of the UV and optical light is probably caused predominantly by dust within the inner core. In the VISIR J7.9 filter image, the central core is resolved in at least three knots (Figure A.1). In the PAH2 and NeII filters, for which we have comparison VISIR images in 2005, this core is unresolved. For an aperture of $0.5''$ radius around the central bright source, we derive $F_{\nu, \text{PAH2}, 2005} = 3130 \pm 50 \text{ Jy}$ and $F_{\nu, \text{NeII}, 2005} = 2710 \pm 180 \text{ Jy}$, compared with $F_{\nu, \text{PAH2}, 2018} = 3140 \pm 10 \text{ Jy}$ and $F_{\nu, \text{NeII}, 2018} = 3200 \pm 30 \text{ Jy}$. Additional systematic errors are about 10%. There appears to be no detectable change in mid-IR flux of the inner core in the last 13 yr. This implies either an equilibrium or very weak dust formation and destruction close to the star. If the geometry of this central knot would simply expand, then the optical depth $\tau(\text{UV}, \text{optical})$ would decline, depending on grain properties (chemistry, shape, size). In this case, and if $\tau(\text{IR}) < 1$, we would expect a small effect ($< 2-10\%$ depending on wavelength and hidden in the uncertainties) in the integrated mid-IR flux since the IR emission is determined by the larger nebula. Any stochastic increase or decrease in line-of-sight dust changes the UV and optical extinction instantly, but not the IR emission as the dust particles are heated and will radiate.

3.3. Resolved dusty circumstellar structures

Several authors have suggested a disk-, ring-, or torus-like structure of $5 - 6''$ in diameter around the central star, which absorbs, scatters, and re-radiates the stellar radiation in the IR (Gehrz et al. 1973, Sutton et al. 1974, Hyland et al. 1979, Warren-Smith et al. 1978, Rigaut & Gehring 1995, Smith et al. 1995, Polomski et al. 1999). Morris et al. (1999) show that most of the dust in the equatorial region is located in toroidal structures, probably created in shock-heated gas of the 19th century eruption. Some

dust may also be located in an inner unresolved torus or disk and/or pinwheel-like structures created by colliding winds in the orbital plane (Weigelt et al. 2016). Smith et al. (2002) present mid-IR images from 4.8–24.5 μm which support the presence of a circumstellar torus or disk. Artigau et al. (2011) argue that this “Butterfly” nebula (Chesneau et al. 2005) is not a coherent physical structure or equatorial torus but spatially separate clumps and filaments ejected at different times. Radial velocity information from ALMA observations support the general picture that the loops are a pinched torus in the orbital plane, perpendicular to the Homunculus lobes (Smith et al. 2018). The direction of the pinched material matches periastron/apastron orientation (Madura et al. 2013) and the companion may have played a role in disrupting the torus soon after its ejection.

The geometry of the dust surrounding η Car is quite complex, see Figure 1 (also Smith et al. 2002). In the center, two bright ring-like structures form the “Butterfly” nebula. Most of the dust is located in this central region (50% of the flux originates within a 3'' radius from the central source, 80% within a 5'' radius). In the mid-IR, one can identify strong density or temperature gradients and knots along these loops, but also spatially coherent structures.

Comparison between the 2005 and 2018 VISIR images show that the two prominent loops are expanding at a rate of up to 0.01'' yr⁻¹ projected on sky. This corresponds to projected velocities of $\sim 100 \text{ km s}^{-1}$ at a distance of 2.3 kpc, consistent with velocities in the equatorial plane (Davidson et al. 2001). The rings seem to expand without losing their overall appearance, in support of physically coherent structures. The furthest extent of the “Butterfly” nebula is about 2'' from the central source, which points toward an ejection during or in the decades before the 19th century eruption. We do not find any brightness changes of the inner loop-like structures between observations separated by 13 years. For an aperture of 3'' radius, we derive $F_{\nu, \text{PAH2}, 2005} = 34170 \pm 520 \text{ Jy}$ and $F_{\nu, \text{NeII}, 2005} = 30100 \pm 2010 \text{ Jy}$, compared with $F_{\nu, \text{PAH2}, 2018} = 34500 \pm 150 \text{ Jy}$ and $F_{\nu, \text{NeII}, 2018} = 32020 \pm 280 \text{ Jy}$. The response time for the dust formation or destruction at these distances from the star is not clear. However, the constant flux and overall appearance of these loops may imply that there is no recent dust formation or destruction and the material is simply expanding, as these structures are likely optically thin.

Clues to the history and origin of η Car’s mass ejection phases can be found in its circumstellar material. Hydrodynamical simulations show that a spherical mass ejection into a massive pre-existing torus of gas and dust could result in the present-day bi-polar geometry of the Homunculus nebula (Frank et al. 1995, Dwarkadas & Balick 1998). The massive torus may have been created shortly before the 19th century eruption, e.g., through non-conservative mass transfer, leaving an unstable core that then erupted.

4. Conclusions

The mid-IR flux densities of η Car’s Homunculus nebula from 8–20 μm show no long-term decline since the first available mid-IR photometry in 1968. Eta Car’s luminosity has thus probably been stable over the last five decades ($\sim 4.6 \times 10^6 L_{\odot}$, adopting a distance of 2.3 kpc). Mid-IR observations were obtained irregularly and at different orbital phases. The large uncertainties of the mid-IR photometry (10% in N band and 20% in Q band) prohibits the confirmation of smaller short-term fluctuations or variations with the orbital period.

Contrary to previous publications, we find no long-term decline of mid-IR photometric levels, which would have indicated a reduction in circumstellar extinction and could have explained the increase in UV and optical brightness. The most likely scenario to explain η Car’s brightening at UV and optical wavelengths, and its stability in the mid-IR, is that the extinction caused by circumstellar dust is declining in our line-of-sight only.

Acknowledgements. We thank the anonymous referee for the constructive feedback. MJB acknowledges support from ERC grant SNDUST 694520. We have used SketchAndCalc to calculate the areas in isophotal contour maps (E. M. Dobbs; www.SketchAndCalc.com).

References

- Aitken, D. K. & Jones, B. 1975, *MNRAS*, 172, 141
 Artigau, É., Martin, J. C., Humphreys, R. M., et al. 2011, *AJ*, 141, 202
 Chesneau, O., Min, M., Herbst, T., et al. 2005, *A&A*, 435, 1043
 Cohen, M., Walker, R. G., Carter, B., et al. 1999, *AJ*, 117, 1864
 Conti, P. S. 1984, in *IAU Symposium*, Vol. 105, *Observational Tests of the Stellar Evolution Theory*, ed. A. Maeder & A. Renzini, 233
 Conti, P. S. 1997, in *PASPC*, Vol. 120, *Luminous Blue Variables: Massive Stars in Transition*, ed. A. Nota & H. Lamers, 387
 Cox, P., Mezger, P. G., Sievers, A., et al. 1995, *A&A*, 297, 168
 Damineli, A., Conti, P. S., & Lopes, D. F. 1997, *New Astronomy*, 2, 107
 Damineli, A., Fernández-Lajús, E., Almeida, L. A., et al. 2019, *MNRAS*, 484, 1325
 Davidson, K. 1971, *MNRAS*, 154, 415
 Davidson, K., Gull, T. R., Humphreys, R. M., et al. 1999, *AJ*, 118, 1777
 Davidson, K., Helmel, G., & Humphreys, R. M. 2018a, *RNAAS*, 2, 133
 Davidson, K. & Humphreys, R. M. 1997, *ARA&A*, 35, 1
 Davidson, K. & Humphreys, R. M., eds. 2012, *ASSL*, Vol. 384, *Eta Carinae and the Supernova Impostors*
 Davidson, K., Ishibashi, K., Martin, J. C., & Humphreys, R. M. 2018b, *ApJ*, 858, 109
 Davidson, K., Martin, J., Humphreys, R. M., et al. 2005, *AJ*, 129, 900
 Davidson, K. & Ostriker, J. P. 1972, *Nature Physical Science*, 236, 46
 Davidson, K., Smith, N., Gull, T. R., Ishibashi, K., & Hillier, D. J. 2001, *AJ*, 121, 1569
 Dwarkadas, V. V. & Balick, B. 1998, *AJ*, 116, 829
 Frank, A., Balick, B., & Davidson, K. 1995, *ApJ*, 441, L77
 Frew, D. J. 2004, *Journal of Astronomical Data*, 10
 Gal-Yam, A. & Leonard, D. C. 2009, *Nature*, 458, 865
 Gehrz, R. D., Ney, E. P., Becklin, E. E., & Neugebauer, G. 1973, *Astrophys. Lett.*, 13, 89
 Gomez, H. L., Vlahakis, C., Stretch, C. M., et al. 2010, *MNRAS*, 401, L48
 Groh, J. H., Meynet, G., & Ekström, S. 2013, *A&A*, 550, L7
 Hackwell, J. A., Gehrz, R. D., & Grasdalen, G. L. 1986, *ApJ*, 311, 380
 Harvey, P. M., Hoffmann, W. F., & Campbell, M. F. 1978, *A&A*, 70, 165
 Hillier, D. J. & Allen, D. A. 1992, *A&A*, 262, 153
 Humphreys, R. M. & Davidson, K. 1994, *PASP*, 106, 1025
 Hyland, A. R., Robinson, G., Mitchell, R. M., Thomas, J. A., & Becklin, E. E. 1979, *ApJ*, 233, 145
 Käufel, H. U., Kerber, F., Asmus, D., et al. 2015, *The Messenger*, 159, 15
 Kessler, M. F., Steinz, J. A., Anderegg, M. E., et al. 1996, *A&A*, 315, L27
 Kotak, R. & Vink, J. S. 2006, *A&A*, 460, L5
 Lagage, P. O., Pel, J. W., Authier, M., et al. 2004, *The Messenger*, 117, 12
 Langer, N., Hamann, W.-R., Lennon, M., et al. 1994, *A&A*, 290, 819
 Madura, T. I., Gull, T. R., Okazaki, A. T., et al. 2013, *MNRAS*, 436, 3820
 Maeder, A. 1983, *A&A*, 120, 113
 Martin, J. C., Davidson, K., & Koppelman, M. D. 2006, *AJ*, 132, 2717
 Mehner, A., Davidson, K., Ferland, G. J., & Humphreys, R. M. 2010, *ApJ*, 710, 729
 Mehner, A., Ishibashi, K., Whitelock, P., et al. 2014, *A&A*, 564, A14
 Morris, P. W., Gull, T. R., Hillier, D. J., et al. 2017, *ApJ*, 842, 79
 Morris, P. W., Waters, L. B. F. M., Barlow, M. J., et al. 1999, *Nature*, 402, 502
 Neugebauer, G. & Westphal, J. A. 1968, *ApJ*, 152, L89
 Nota, A. & Lamers, H., eds. 1997, *ASPC*, Vol. 120, *Luminous Blue Variables: Massive Stars in Transition*
 Pagel, B. E. T. 1969, *Astrophys. Lett.*, 4, 221
 Polomski, E. F., Telesco, C. M., Piña, R. K., & Fisher, R. S. 1999, *AJ*, 118, 2369
 Reimann, H.-G., Linz, H., Wagner, R., et al. 2000, in *Proc. SPIE*, Vol. 4008, *Optical and IR Telescope Instrumentation and Detectors*, ed. M. Iye & A. F. Moorwood, 1132–1143

- Rigaut, F. & Gehring, G. 1995, in RMxAA, vol. 27, Vol. 2, RMxAA Conf. Ser., ed. V. Niemela, N. Morrell, & A. Feinstein, 27–35
- Robinson, G., Hyland, A. R., & Thomas, J. A. 1973, MNRAS, 161, 281
- Russell, R. W., Lynch, D. K., Hackwell, J. A., et al. 1987, ApJ, 321, 937
- Smith, C. H., Aitken, D. K., Moore, T. J. T., et al. 1995, MNRAS, 273, 354
- Smith, N., Gehrz, R. D., Hinz, P. M., et al. 2003, AJ, 125, 1458
- Smith, N., Gehrz, R. D., Hinz, P. M., et al. 2002, ApJ, 567, L77
- Smith, N., Ginsburg, A., & Bally, J. 2018, MNRAS, 474, 4988
- Smith, N., Li, W., Foley, R. J., et al. 2007, ApJ, 666, 1116
- Sutton, E., Becklin, E. E., & Neugebauer, G. 1974, ApJ, 190, L69
- Trundle, C., Kotak, R., Vink, J. S., & Meikle, W. P. S. 2008, A&A, 483, L47
- Van Malderen, R., Decin, L., Kester, D., et al. 2004, A&A, 414, 677
- Warren-Smith, R. F., Scarrot, S. M., Murdin, P., & Bingham, R. G. 1978, Memorie della Societa Astronomica Italiana, 49, 589
- Weigelt, G., Albrecht, R., Barbieri, C., et al. 1995, in RMxAA, vol. 27, Vol. 2, RMxAA Conf. Ser., ed. V. Niemela, N. Morrell, & A. Feinstein, 11
- Weigelt, G. & Ebersberger, J. 1986, A&A, 163, L5
- Weigelt, G., Hofmann, K.-H., Schertl, D., et al. 2016, A&A, 594, A106
- Westphal, J. A. & Neugebauer, G. 1969, ApJ, 156, L45
- White, S. M., Duncan, R. A., Chapman, J. M., & Koribalski, B. 2005, in ASP Conf. Ser., Vol. 332, The Fate of the Most Massive Stars, ed. R. Humphreys & K. Stanek, 129
- Whitelock, P. A., Feast, M. W., Marang, F., & Breedt, E. 2004, MNRAS, 352, 447

Appendix A: Mid-IR images with VISIR in 2018

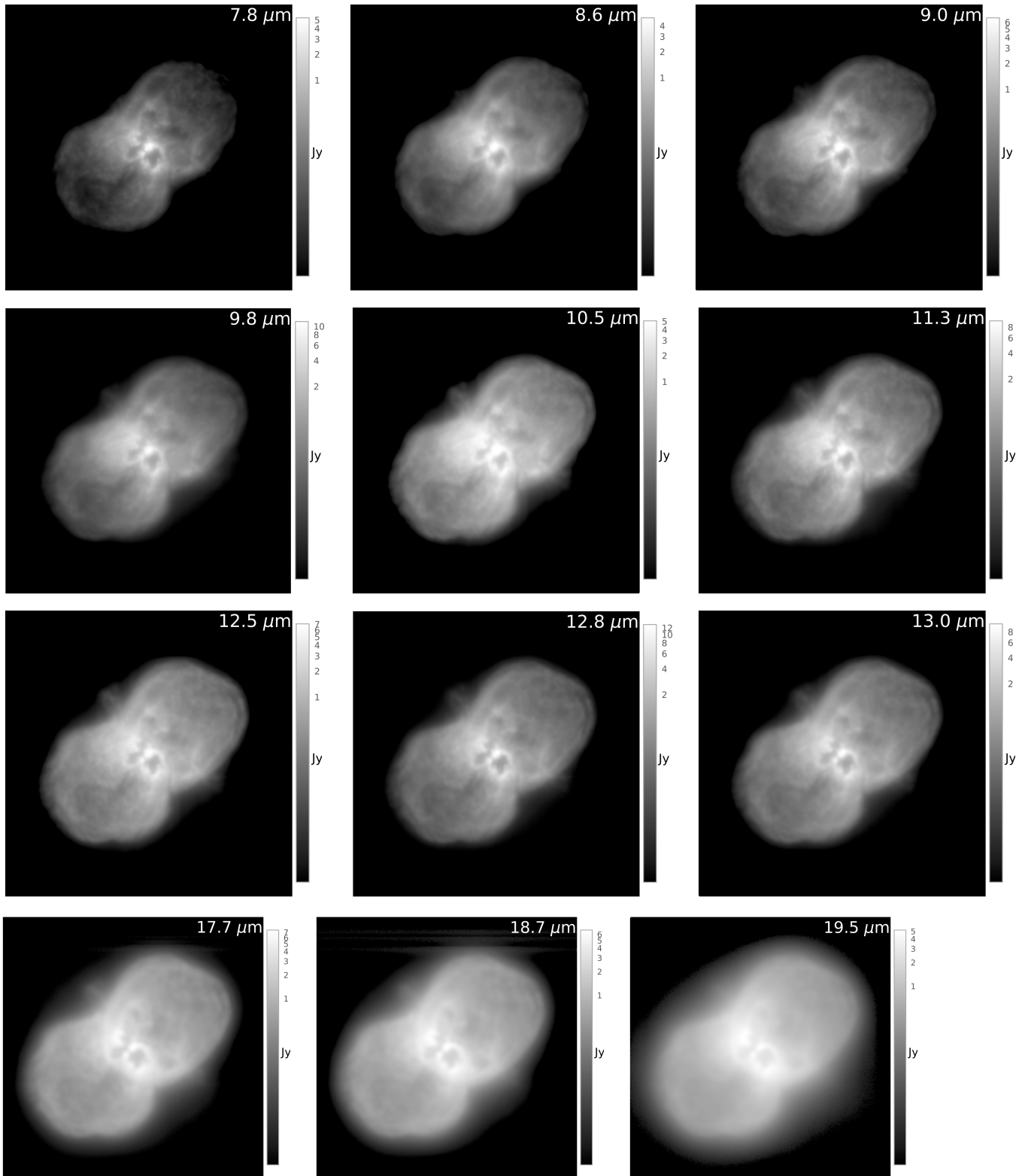


Fig. A.1: VISIR 2018 images of η Car's Homunculus nebula. The flux density in Jy per detector pixel ($0.045''/\text{pixel}$) is shown on a logarithmic scale. The *N*-band images have a field-of-view of $25'' \times 25''$, the *Q*-band images (last row) of $22.5'' \times 22.5''$.

Appendix B: Journal of VISIR and TIMMI2 observations

Table B.1: Journal of VISIR observations.

Date	MJD	Target	Filter	Wavelength (μm)	Image quality ($''$)	ESO PROG.ID
2005-01-23	53393.05	HD9138	PAH2	11.25	0.39	074.A-9016(A); PI: Lagage
2005-01-23	53393.10	HD59294	PAH2	11.25	0.36	074.A-9016(A)
2005-01-23	53393.18	HD30080	NEII	12.81	0.38	074.A-9016(A)
2005-01-23	53393.25	HD62902	NEII	12.81	0.38	074.A-9016(A)
2005-01-23	53393.37	eta Car	NEII	12.81	0.38	074.A-9016(A)
2005-01-23	53393.37	eta Car	PAH2	11.25	0.37	074.A-9016(A)
2018-04-28	58237.00	eta Car	PAH1	8.59	0.23	0101.D-0077(A); PI: Mehner
2018-04-29	58237.00	eta Car	SIV	10.49	0.27	0101.D-0077(A)
2018-04-29	58237.00	eta Car	B12.4	12.47	0.31	0101.D-0077(A)
2018-04-29	58237.01	HD89682	PAH1	8.59	0.23	0101.D-0077(A)
2018-04-29	58237.02	HD89682	SIV	10.49	0.27	0101.D-0077(A)
2018-04-29	58237.02	HD89682	B12.4	12.47	0.31	0101.D-0077(A)
2018-05-11	58249.10	eta Car	Q1	17.65	~0.50	0101.D-0077(A)
2018-05-11	58249.11	eta Car	Q2	18.72	~0.50	0101.D-0077(A)
2018-05-11	58249.12	eta Car	Q3	19.50	~0.50	0101.D-0077(A)
2018-05-11	58249.13	HD89682	Q1	17.65	~0.50	0101.D-0077(A)
2018-05-11	58249.13	HD89682	Q2	18.72	~0.50	0101.D-0077(A)
2018-05-11	58249.14	HD89682	Q3	19.50	~0.50	0101.D-0077(A)
2018-05-21	58259.97	eta Car	J7.9	7.78	0.22	0101.D-0077(A)
2018-05-21	58259.98	eta Car	SIV_1	9.82	0.31	0101.D-0077(A)
2018-05-21	58259.99	HD89682	J7.9	7.78	0.22	0101.D-0077(A)
2018-05-21	58260.00	HD89682	SIV_1	9.82	0.31	0101.D-0077(A)
2018-12-10	58462.31	eta Car	ARIII	8.99	0.26	0101.D-0077(A)
2018-12-10	58462.31	eta Car	PAH2	11.25	0.29	0101.D-0077(A)
2018-12-10	58462.32	eta Car	NEII	12.81	0.33	0101.D-0077(A)
2018-12-10	58462.32	eta Car	NEII_2	13.04	0.33	0101.D-0077(A)
2018-12-10	58462.33	HD89682	ARIII	8.99	0.26	0101.D-0077(A)
2018-12-10	58462.34	HD89682	PAH2	11.25	0.29	0101.D-0077(A)
2018-12-10	58462.34	HD89682	NEII	12.81	0.33	0101.D-0077(A)
2018-12-10	58462.35	HD89682	NEII_2	13.04	0.33	0101.D-0077(A)

Table B.2: Journal of TIMMI2 observations.

Date	MJD	Target	Filter	Wavelength (μm)	ESO PROG.ID
2003-01-26	52665.26	HD81797	N10.4	10.3	60.A-9126(C); Engineering run
2003-01-26	52665.26	HD81797	N11.9	11.6	60.A-9126(C)
2003-01-26	52665.26	HD81797	N10.4	10.3	60.A-9126(C)
2003-01-26	52665.27	HD81797	N11.9	11.6	60.A-9126(C)
2003-01-26	52665.27	HD81797	Q1	17.8	60.A-9126(C)
2003-01-26	52665.29	eta Car	N7.9	7.9	60.A-9126(C)
2003-01-26	52665.30	eta Car	N8.9	8.7	60.A-9126(C)
2003-01-26	52665.30	eta Car	N10.4	10.3	60.A-9126(C)
2003-01-26	52665.3	eta Car	N11.9	11.6	60.A-9126(C)
2003-01-26	52665.31	eta Car	N12.9	12.3	60.A-9126(C)
2003-01-26	52665.32	eta Car	[NeII]	12.8	60.A-9126(C)
2003-01-26	52665.32	eta Car	Q1	17.8	60.A-9126(C)
2003-01-26	52665.33	eta Car	N9.8	9.6	60.A-9126(C)
2003-01-26	52665.33	eta Car	N9.8	9.6	60.A-9126(C)
2003-01-26	52665.34	HD81797	N7.9	7.9	60.A-9126(C)
2003-01-26	52665.35	HD81797	N8.9	8.7	60.A-9126(C)
2003-01-26	52665.35	HD81797	N9.8	9.6	60.A-9126(C)
2003-01-26	52665.35	HD81797	N10.4	10.3	60.A-9126(C)
2003-01-26	52665.35	HD81797	N11.9	11.6	60.A-9126(C)
2003-01-26	52665.35	HD81797	N12.9	12.3	60.A-9126(C)
2003-01-26	52665.36	HD81797	[NeII]	12.8	60.A-9126(C)
2003-01-26	52665.36	HD81797	Q1	17.8	60.A-9126(C)
2003-03-19	52717.45	HD156277	N10.4	10.3	60.A-9126(E); Engineering run
2003-03-19	52717.45	HD156277	[NeII]	12.8	60.A-9126(E)
2003-05-14	52773.07	HD123139	N10.4	10.3	60.A-9126(A); Engineering run
2003-05-14	52773.07	HD123139	N9.8	9.6	60.A-9126(A)
2003-05-14	52773.08	HD123139	N8.9	8.7	60.A-9126(A)
2003-05-14	52773.08	HD123139	N7.9	7.9	60.A-9126(A)
2003-05-14	52773.08	HD123139	N12.9	12.3	60.A-9126(A)
2003-05-14	52773.09	HD123139	[NeII]	12.8	60.A-9126(A)
2003-05-14	52773.10	HD123139	M	4.6	60.A-9126(A)
2003-05-14	52773.12	eta Car	N7.9	7.9	60.A-9126(I); Engineering run
2003-05-14	52773.12	eta Car	N7.9	7.9	60.A-9126(I)
2003-05-14	52773.12	eta Car	N8.9	8.7	60.A-9126(I)
2003-05-14	52773.13	eta Car	N10.4	10.3	60.A-9126(I)
2003-05-14	52773.13	eta Car	N12.9	12.3	60.A-9126(I)
2003-05-14	52773.13	eta Car	[NeII]	12.8	60.A-9126(I)
2003-05-14	52773.14	eta Car	M	4.6	60.A-9126(I)
2003-05-14	52773.14	eta Car	N7.9	7.9	60.A-9126(I)
2003-05-14	52773.15	eta Car	N8.9	8.7	60.A-9126(I)
2003-05-14	52773.15	eta Car	N7.9	7.9	60.A-9126(I)
2003-05-14	52773.15	eta Car	N8.9	8.7	60.A-9126(I)
2003-05-14	52773.15	eta Car	N9.8	9.6	60.A-9126(I)
2003-05-14	52773.15	eta Car	N10.4	10.3	60.A-9126(I)
2003-05-14	52773.16	eta Car	N12.9	12.3	60.A-9126(I)
2003-05-14	52773.16	eta Car	[NeII]	12.8	60.A-9126(I)
2003-05-14	52773.16	eta Car	M	4.6	60.A-9126(I)
2003-05-14	52773.96	HD108903	N7.9	7.9	69.D-0304(B); PI: Gehrz
2003-05-14	52773.97	HD108903	N8.9	8.7	69.D-0304(B)
2003-05-14	52773.97	HD108903	N9.8	9.6	69.D-0304(B)
2003-05-14	52773.97	HD108903	N10.4	10.3	69.D-0304(B)
2003-05-14	52773.97	HD108903	N11.9	11.6	69.D-0304(B)
2003-05-14	52773.97	HD108903	Q1	17.8	69.D-0304(B)
2003-05-14	52773.98	HD108903	M	4.6	69.D-0304(B)
2003-05-14	52773.98	eta Car	N7.9	7.9	69.D-0304(B)
2003-05-14	52773.98	eta Car	N8.9	8.7	69.D-0304(B)
2003-05-14	52773.99	eta Car	N9.8	9.6	69.D-0304(B)
2003-05-14	52773.99	eta Car	N10.4	10.3	69.D-0304(B)
2003-05-14	52773.99	eta Car	N11.9	11.6	69.D-0304(B)
2003-05-14	52773.99	eta Car	N11.9	11.6	69.D-0304(B)

Date	MJD	Target	Filter	Wavelength (μm)	ESO PROG.ID
2003-05-14	52774.00	eta Car	N11.9	11.6	69.D-0304(B)
2003-05-15	52774.00	eta Car	Q1	17.8	69.D-0304(B)
2003-05-15	52774.01	eta Car	M	4.6	69.D-0304(B)
2003-05-15	52774.01	eta Car	N8.9	8.7	69.D-0304(B)
2003-05-15	52774.01	eta Car	N11.9	11.6	69.D-0304(B)
2003-05-15	52774.02	eta Car	Q1	17.8	69.D-0304(B)
2003-05-15	52774.94	HD108903	N8.9	8.7	69.D-0304(B)
2003-05-15	52774.94	HD108903	N11.9	11.6	69.D-0304(B)
2003-05-15	52774.95	HD108903	Q1	17.8	69.D-0304(B)
2003-05-15	52774.95	HD108903	M	4.6	69.D-0304(B)
2003-05-15	52774.99	eta Car	N7.9	7.9	69.D-0304(B)
2003-05-15	52774.99	eta Car	N8.9	8.7	69.D-0304(B)
2003-05-15	52775.00	eta Car	N9.8	9.6	69.D-0304(B)
2003-05-15	52775.00	eta Car	N10.4	10.3	69.D-0304(B)
2003-05-15	52775.00	eta Car	N11.9	11.6	69.D-0304(B)
2003-05-16	52775.00	eta Car	N12.9	12.3	69.D-0304(B)
2003-05-16	52775.00	eta Car	[NeII]	12.8	69.D-0304(B)
2003-05-16	52775.01	eta Car	Q1	17.8	69.D-0304(B)
2003-05-16	52775.01	eta Car	M	4.6	69.D-0304(B)
2003-05-16	52775.02	HD108903	N7.9	7.9	69.D-0304(B)
2003-05-16	52775.02	HD108903	N8.9	8.7	69.D-0304(B)
2003-05-16	52775.02	HD108903	N9.8	9.6	69.D-0304(B)
2003-05-16	52775.02	HD108903	N10.4	10.3	69.D-0304(B)
2003-05-16	52775.02	HD108903	N11.9	11.6	69.D-0304(B)
2003-05-16	52775.02	HD108903	N12.9	12.3	69.D-0304(B)
2003-05-16	52775.02	HD108903	[NeII]	12.8	69.D-0304(B)
2003-05-16	52775.03	HD108903	Q1	17.8	69.D-0304(B)
2003-05-16	52775.03	HD108903	M	4.6	69.D-0304(B)
2003-05-27	52786.94	HD110458	N7.9	7.9	71.D-0049(A); PI: Zijlstra
2003-05-27	52786.94	HD110458	N11.9	11.6	71.D-0049(A)
2003-05-27	52786.95	HD110458	N12.9	12.3	71.D-0049(A)
2003-05-27	52786.96	eta Car	N7.9	7.9	71.D-0049(A)
2003-05-27	52786.97	eta Car	N11.9	11.6	71.D-0049(A)
2003-05-27	52786.97	eta Car	N12.9	12.3	71.D-0049(A)